Hindawi
Advances in Materials Science and Engineering
Volume 2022, Article ID 6898455, 13 pages
https://doi.org/10.1155/2022/6898455

Research Article

Study on the Construction Waste Composition and Strength Mechanism of Recycled Mixture

Sanqiang Yang, Zhenyu Yang, and Jie Liu

College of Civil Engineering and Architecture, Hebei University, Baoding 071000, China

Correspondence should be addressed to Zhenyu Yang; yzy32351@163.com

Received 1 September 2022; Revised 5 October 2022; Accepted 20 October 2022; Published 30 October 2022

Academic Editor: Shengwen Tang

Recycling of construction waste has been a hot issue in road engineering research, and microscopic characteristics and composition of construction waste-recycled aggregate (RA) significantly influence their macroscopic service characteristics. In this paper, the composition, microstructure, and strength formation mechanism of natural aggregate (NA), recycled concrete aggregate (RCA), and recycled brick (RCB) were systematically studied by *X*-ray diffraction analysis (XRD), scanning electron microscopy (SEM), fractal dimension and porosity determination, unconfined compressive strength test, and indirect tensile test. The results showed that RA's microscopic morphological characteristics and chemical components were analyzed by combining XRD and SEM electron microscopy techniques. RA has prominent fractal features, and the smaller bulk density and more extensive crushing value index of RA correspond to its larger porosity as well as fractal dimension. The attributes of RA lead to the peak of 7 d unconfined compressive strength and 7 d splitting strength of the mix. The reasonable control of RA admixture benefits the improvement of mix strength. This study relies on engineering to carry out theoretical and experimental research, which provides essential support and guarantee for the application of construction waste in the field of highway transportation in Hebei Province.

1. Introduction

With the rapid progress of industrialization and urbanization in China, the large amount of construction waste generated has become the core problem that needs to be solved in today's urban development. By 2020, China's construction waste output will be as high as 3 billion *t*. Still, the resource utilization rate of construction waste is less than 10%, and the large amount of construction waste has become a severe hidden danger that hinders urban development and pollutes the ecological environment [1]. In this context, the research on the resource utilization of construction waste is urgent. The analysis of the construction waste composition and mix formation mechanism is of great help to better study the macromechanical properties of RA and road performance.

Zhe Li used IPP software to identify CT scan images of construction waste-recycled mixes and analyzed recycled mixtures' microscopic particle morphology and particle contact characteristics [2]. Qi Jianfeng et al. [3] used the IPP image-processing technique for rock microporosity calculation by analyzing the rock micromorphological features of SEM images at different magnifications. Gao Song et al. [4] used fractal theory to quantitatively evaluate recycled sand and recycled mortar and proposed the RA quality evaluation method with fractal dimension as the index. Jangfeng Wu et al. [5] used XRD and SEM techniques to analyze rocks' aggregate morphology and chemical composition and calculated the fractal dimension of different types of stones. Yang Jin [6] studied the fractal dimension of coal gangue and fly ash cement composites with varying dosing levels. The pore structure and microfractal scale were investigated, and it was found that the porosity of blended composites was elevated, and the higher the doping amount, the higher the porosity. The scale of the microfractal region was larger than that of the macrofractal region. Wang Lei [7, 8] investigated the mechanical properties of silica fume-modified low heat silicate cement, fractal characteristics, and the effect of

shrinkage crack resistance of concrete with different fly ash admixtures and found that the pore structure of silica fume-modified low heat silicate cement became more complex and that the fractal dimension value became higher. It can be used as a new parameter to evaluate concrete shrinkage, revealing the effect of fly ash from the perspective of the pore structure and fractal dimension. Wang Yue [9] determined the capillary water absorption of cementitious materials with different water-cement ratios and mineral admixture types and found that the water absorption of cementitious materials was mainly related to the pore size. Capillary water absorption increased continuously with the increase of the pore fractal dimension.

The microscopic morphological characteristics and chemical composition of metals, rocks, concrete, soil, asphalt, and other materials have been studied by SEM images and XRD diffraction tests [10–15], and the pores, fractures, microstructure, and composition of rocks have been studied indirectly by professional image-processing software and chemical analysis software. Researchers have studied the permeability of concrete, the fractal characteristics of fly ash, the influence of magnesium phosphate cement paste pore structure fractal characteristics and hydration simulation, as well as the different alkali sulfate on low-heat Portland cement, the heat Portland cement and ordinary Portland cement shrinkage, hydration, pore structure, fractal dimension, and the influence of the microstructure [16–23]. This inspired researchers to analyze the compositional composition of RA by XRD diffraction tests. Based on scanning electron microscopy tests, the Image *J* professional image-processing technique was applied to obtain RA's microscopic pore structure characteristic parameters. The box-counting method was used to calculate the fractal dimension of different types of RA and combined with the indoor tests to analyze the strength formation mechanism of recycled mixes. This is of great importance to improve the utilization rate of construction waste resource utilization.

2. Materials and Methods

2.1. Materials. NA used in this test is 0~5.0 mm, 5.0~10.0 mm, 10~20 mm, and 20~30 mm aggregates produced by a stone plant in Mancheng County, Baoding City, Hebei Province, whose main rock components are limestone and granite. The material source of construction waste is obtained from old buildings demolished in the central city of Baoding, and the processing process of "jaw crushing + manual sorting + magnetic separation + impact crushing + screening + washing" is adopted. As shown in Figure 1, the RA of construction waste after crushing and sorting is mainly RCA and RCB.

The cement is made of Shijiazhuang Quzhai ordinary Portland cement, the strength grade is 42.5, and the cement properties meet the requirements of JTJ 034 specification. RA uses 5̃10mm, 10̃20mm RCA and 0̃5mm, 10̃20mm RCB produced by Baoding Lvsheng Environmental Technology Company. A gauge removed flat and elongated particles in the coarse aggregate, and the sum was kept in an oven at 110°C for four *h* to make it completely dry. The entirety was taken out after cooling. According to the relevant requirements of the "Highway Engineering Aggregate Test Rules" (JTG E30-2005) and "Highway Pavement Base Construction Technical Rules" (JTG/T F20-2015), raw materials are tested, as shown in Table 1.

2.2. Scanning Electron Microscope Test. NA, RCA, and RCB were selected as research objects, and the elemental composition of aggregates was determined by using a Feiner desktop scanning electron microscope using *X*-ray energy spectrometry (EDS) analysis with a processing capacity of 2048 channels @ 10ev/ch multichannel analysis, and 10 KV was selected as the accelerating voltage for the test. For RA and NA respectively, the elemental composition of aggregates was analyzed by the three-point analysis method; i.e., three different points were selected in the same graph. The elemental content ratio of the three points was analyzed by *X*-ray energy spectrometry to reduce the error of the analysis and improve the credibility of the analysis results. The microstructure of NA at different magnifications of 10,000×, 15,000×, and 20,000× was also used to calculate the porosity and fractal dimension using ImageJ software.

2.3. X-Ray Diffraction Test. The XRD diffraction test was performed using a D8 DISCOVER Plus diffractometer from Bruker AXS, Germany. First, small pieces of RCA, RCB, and NA specimens were ground to a powder form with a mortar, and the models were pressed and made into samples by the positive pressure method to produce three test samples. The test samples were put into the *X*-ray diffractometer, and phase matching and result analysis were performed using Jade 6.0 software.

2.4. Strength Test of Cement-Stabilized Recycled Mixture. Relying on the provincial highway, S524 Xiong'an New Area to Baoding highway regenerative cement stabilization base experimental section project, the best water content, maximum dry density, 7 d unconfined compressive strength, and 7 d splitting tests were determined for the recycled mix with different doping and cement dosing. The C–B-3 grade recommended in the Technical Rules for Construction of the Road Pavement Base (JTG/T F20-2015) was used, and 0%, 20%, 40%, 60%, 80%, and 100% of RA and 4%, 5%, and 6% of cement mixture were tested according to the Test Procedure for Inorganic Binding Material Stabilization of Highway Engineering (JTGE51-2009). According to the compaction test results, 150 mm × 150 mm cylindrical specimens with 98% compaction were formed by the static compression method, and the unconfined compressive strength test and the splitting test were conducted after 7 d curing, as shown in Figure 2.

3. Results

3.1. Elemental Composition Analysis of X-Ray Energy Spectrum. The test results after energy spectrum analysis are shown in Figures 3, 4 and Tables 2, 3, 4.

(a) (b)

Figure 1: Construction waste and recycling equipment: (a) Construction waste and (b) recycling equipment.

Table 1: Technical indexes of aggregate raw materials.

Indicators	Crushed stone value	Apparent density (g/cm^3)	Saturated surface dry density (g/cm^3)	Bulk density (g/cm^3)	Bibulous rate (%)	Flat and elongated particles in coarse aggregates (%)	Dust content below 0.075 (%)	Content of soft rock (%)
Natural aggregate	18.8	2.778	2.770	2.765	0.164	0.13	0.5	0.8
RCA	21.2	2.547	2.461	2.406	3.299	1.86	1.1	1.6
RCB	37.2	2.134	1.871	1.640	14.115	3.62	1.4	2.2
Specification values	≤26	——	——	——	——	≤18	≤1.2	≤3

Through the EDS analysis of NA and RA, it is found that the element content is O, followed by C, Ca, Si, and other elements. In RCA, for example, O is more than three times as much as C, and more than twice as much as Si. Mg is more than three times as much as Fe. Therefore, it can be inferred that the main components of RCA may be SiO_2, $CaCO_3$, $CaMg(CO_3)_2$, and $CaMg_{0.77}Fe_{0.23}$ $(CO_3)_2$. There will inevitably be other impurities in the electron microscope sample preparation process, which will affect the analytical results.

3.2. X-Ray Diffraction (XRD) Phase Detection. Each crystalline substance has its unique *X*-ray diffraction results, which will not be changed by doping other substances. Therefore, even if the sample is a multiphase mixture, each component will have its diffraction peak on the diffraction pattern. The *D* value and the diffraction pattern's relative intensity I/I1 value were used to identify the mineral composition in the sample. According to this principle, the raw file generated by the test results is imported into Jade 6.0 software and the sample map is compared with the "standard card" in the PDF card after given retrieval conditions, and then, the existence of such a phase is determined according to its peak position, peak strength, and elements in the sample [11, 12]. The X-ray diffraction patterns of RCA, RCB, and NA of construction waste are shown in Figure 5.

It can be seen from Figure 5 that the natural aggregate is mainly composed of limestone ($CaCO_3$) and dolomite ($CaMg(CO_3)_2$). The main components of RCA are silica (SiO_2), calcium carbonate ($CaCO_3$), dolomite ($CaMg(CO_3)_2$), and ferric magnesite ($CaMg_{0.77}Fe_{0.23}(CO_3)_2$). Among them, RCB mainly consists of silicon oxide (SiO_2), magnesium aluminate ($MgAl_2O_4$), magnesium acetate ($C_4H_6MgO_4$), and m-acetanilide ($C_8H_{10}N_2O$). Of construction waste in the process of storage and landfill, due to fermentation and rain erosion, weathered for a long time, harmful material waste such as paint and asphalt produces a series of physical, chemical, and biological reactions, causing the construction waste can create all kinds of poisonous and harmful substances, which will cause severe pollution and harm to soil and water resources. Due to various substances in construction waste, sampling powder for the XRD test leads to many miscellaneous peaks in the XRD pattern.

Taking RCA as an example, four-phase SiO_2, $CaCO_3$, $CaMg(CO_3)_2$, and $CaMg_{0.77}Fe_{0.23}$ $(CO_3)_2$ were selected by phase analysis. The phase analysis results and crystal structure parameters of RCA are shown in Table 5 and Figure 6. The grain size is 31 nm, and the microscopic strain is 0.20%. The lattice parameters are obtained, which lays the foundation for constructing the tiny lattice model.

3.3. Quantitative Characterization and Evaluation of RA Pore Structure. ImageJ is Java-based public image-processing software developed by the National Institutes of Health (NIH) company in the United States. Presently, researchers at home and abroad mainly use ImageJ software for quantitative analysis of aggregates and pores of soil medium

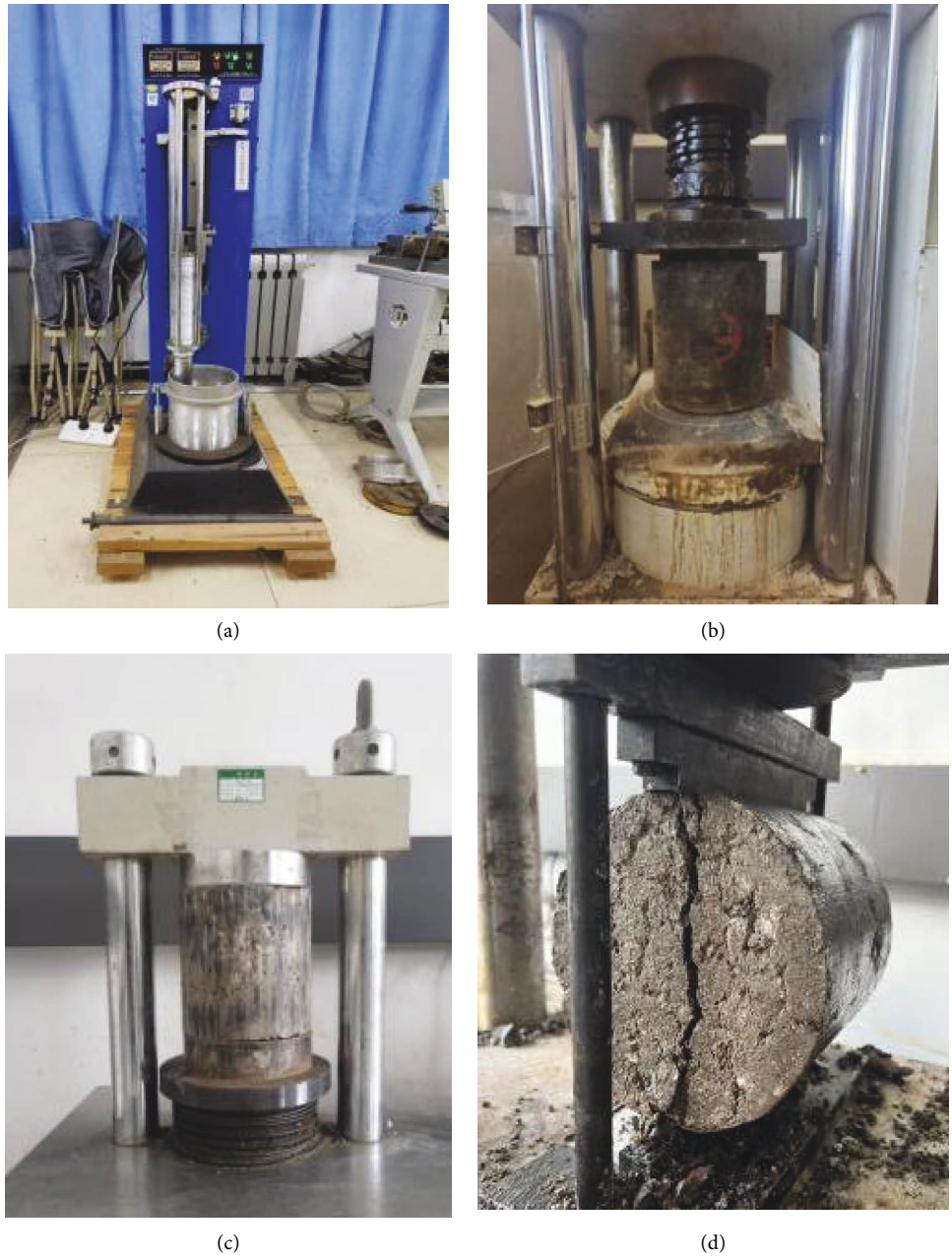

Figure 2: Performance test of the recycled mixture. (a) Compaction test, (b) specimen compaction, (c) unconfined compression test, and (d) Splitting test.

and rock. ImageJ software can be used to quantitatively analyze the related parameters of the processed images, including porosity, equivalent diameter, flatness, and global contour coefficient.

The quantitative evaluation of the pore structure of RA by using ImageJ software mainly includes the following three steps: (1) Correction of the scale: ImageJ's default unit length is pixels, so you need to modify the scale to measure the actual length information. (2) Image binarization processing: Gray images are divided into 256 levels. 0–255 represents different gray values. In the binarization image, 0 illustrates black and 1 illustrates white. Image binarization is a process in which the gray matter of 0–255 in the drawing image is represented by 0 or 1. The gray image function is the input, and the binary operation is the output. The calculation formula is as follows:

$$g(x, y) = \begin{cases} 0, & g(x, y) < T; \\ 1, & g(x, y) \geq T, \end{cases} \tag{1}$$

where T is a threshold.

SEM images and binarized images of recycled aggregates are shown in Figures. 7 and 8.

(3) We calculate microstructure parameters, porosity, pore diameter, etc.

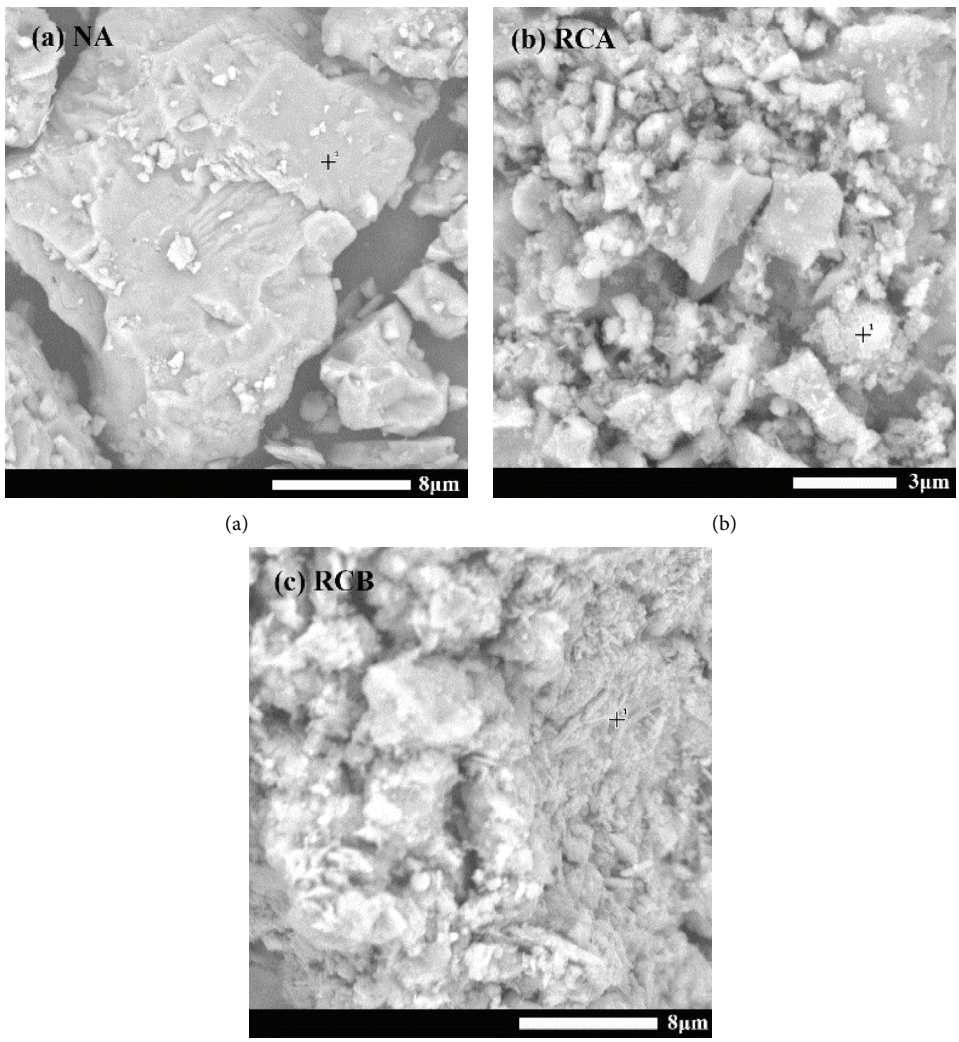

(a) (b)

(c)

Figure 3: Location of EDS.

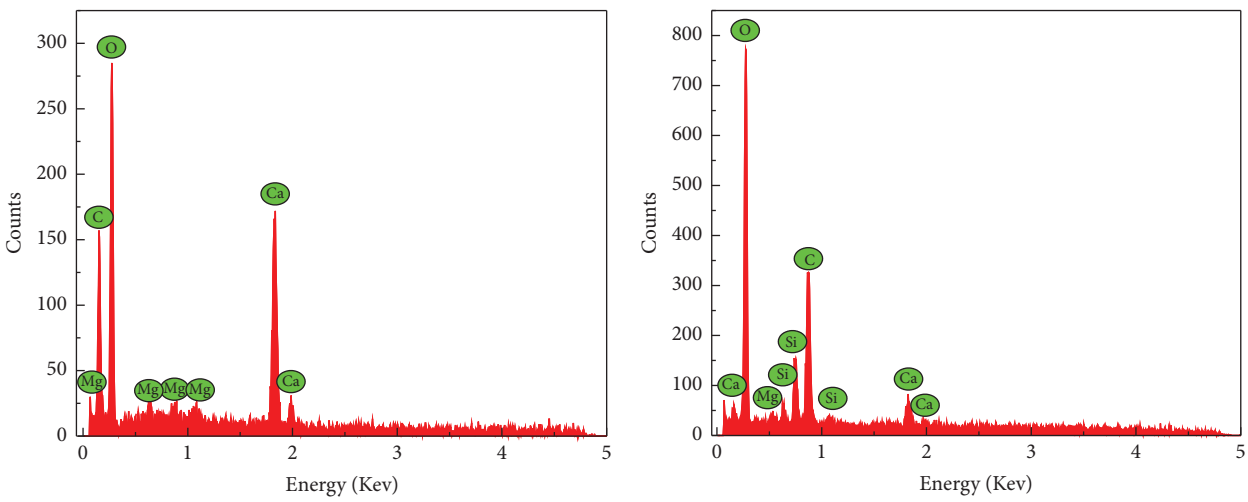

(a) (b)

Figure 4: Continued.

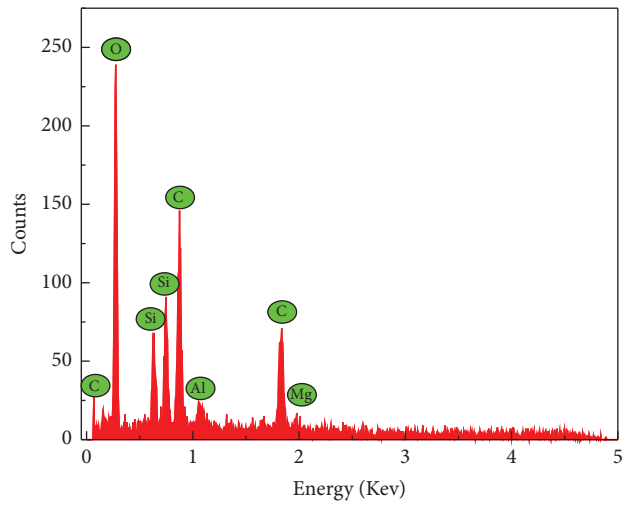

(c)

Figure 4: EDS analysis of RA and NA. (a) Natural aggregates, (b) RCA, and (c) RCB.

Table 2: Elemental composition and content of NA obtained by *X*-ray energy spectrum analysis.

Elements	No.1 weight	No.2 weight	No.3 weight	Average weight	No.1 atomic	No.1 atomic	No.1 atomic	Average atomic
O	64.13	65.96	62.22	64.1	76.15	77.35	74.39	75.96
Ca	29.34	27.47	31.98	29.59	13.91	14.06	15.63	14.53
C	5.14	5.29	5.11	5.17	7.5	5.64	6.72	6.61
Mg	1.39	1.28	0.69	1.12	2.44	2.95	3.26	2.88

Table 3: Elemental composition and content of RCA obtained by X-ray energy spectrum analysis.

Element	No.1 weight	No.2 weight	No.3 weight	Average weight	No.1 atomic	No.1 atomic	No.1 atomic	Average atomic
O	68.34	70.02	72.94	70.43	83.38	79.45	89.12	83.99
C	14.13	14.72	12.56	13.8	9.8	8.77	7.24	8.6
Si	9.88	8.41	7.63	8.64	2.66	5.31	1.46	3.14
Ca	5.48	5.77	4.9	5.38	2.41	3.23	1.29	2.31
Mg	1.63	0.81	1.48	1.31	1.31	2.43	0.67	1.47
Fe	0.54	0.27	0.49	0.44	0.44	0.81	0.22	0.49

Table 4: Elemental composition and content of RCB obtained by X-ray energy spectrum analysis.

Elements	No.1 weight	No.2 weight	No.3 weight	Average weight	No.1 atomic	No.1 atomic	No.1 atomic	Average atomic
O	53.8	54.88	55.44	54.7	73.86	75.93	72.7	74.16
C	13.9	14.36	14.22	14.16	8.12	6.47	7.79	7.46
Si	10.18	9.72	9.23	9.71	7.28	7.81	8.65	7.91
Al	8.73	8.54	8.01	8.43	4.94	5.23	6.08	5.42
Mg	6.87	5.26	6.86	6.33	2.98	2.31	2.54	2.61
H	5.13	5.91	5.1	5.38	2.34	2.22	1.99	2.18
N	1.4	1.33	1.14	1.29	0.49	0.03	0.25	0.26

The abovementioned methods were used to calculate the porosity of the RA microstructure under SEM with large multiples of 10000×, 15000×, and 20000×, respectively, and the results are shown in Table 6.

It can be seen from Table 6 that the porosity of RA is in the order of RCB > RCA > NA. The porosity of RCB is 1.3 times that of RCA and 2.32 times that of NA. The porosity of RA is higher than that of NA, mainly due to the processing and production mode and secondary crushing during regeneration, resulting in many cracks and micropores on its surface and inside. The increase in porosity also reduces the performance of raw materials, resulting in the crushing value, water absorption, and density of construction waste being much higher than those of NA. Finally, its strength, stiffness, and durability are weakened to varying degrees when used in recycled mixtures. Moreover, the porosity of SEM images with different magnifications analyzed by using ImageJ software is different, which may be due to the following reasons: (1) When image binarization is carried out, the threshold is selected according to the naked eye.

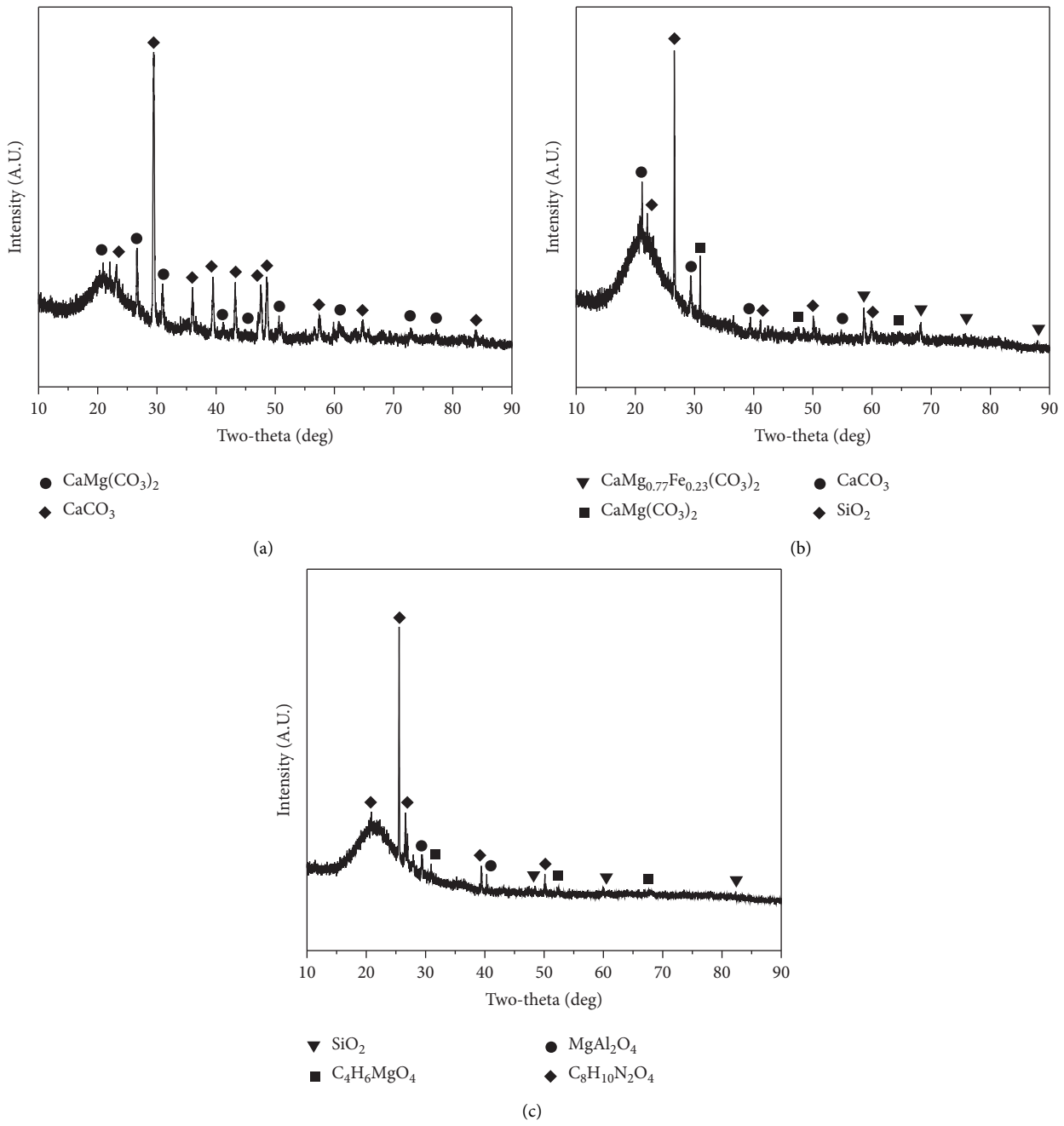

Figure 5: XRD patterns of RA and NA. (a) Natural aggregates, (b) RCA, and (c) RCB.

Table 5: Phase analysis results and cell volume parameters of RCA.

NO	Molecular formula	FOM	PDF-#	J	I%	a	B	C
1	Quartz SiO_2	1.0	86–1630	C	97	4.911	4.911	5.407
2	Calcite $CaCO_3$	4.4	99–0022	+	15	4.989	4.989	17.062
3	Dolomite							
$CaMg(CO_3)_2$	4.2	71–1662	C	20	4.803	4.803	15.984	
4	Dolomite							
$CaMg_{0.77}Fe_{0.23}(CO_3)_2$	5.3	84–2065	C	20	4.812	4.812	16.042	

Different entries will produce different binarization images. (2) Due to different magnifications, different SEM images are selected, resulting in a deviation between the porosity of RA in different areas. (3) The field of view of an SEM electron microscope is different with different magnifications, and the field of view of an SEM electron microscope with large

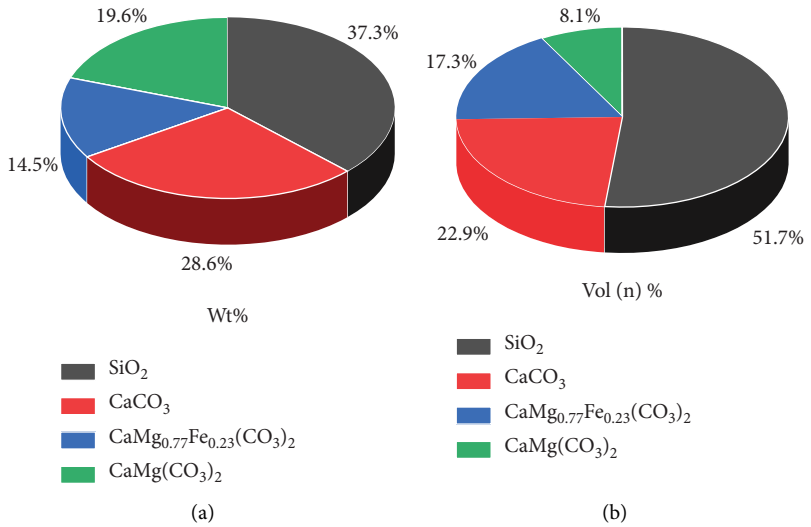

Figure 6: Wt% and vol (n) % of RCA. (a) Relative mass fraction of RCA mineral components. (b) Vol (n) % of RCA.

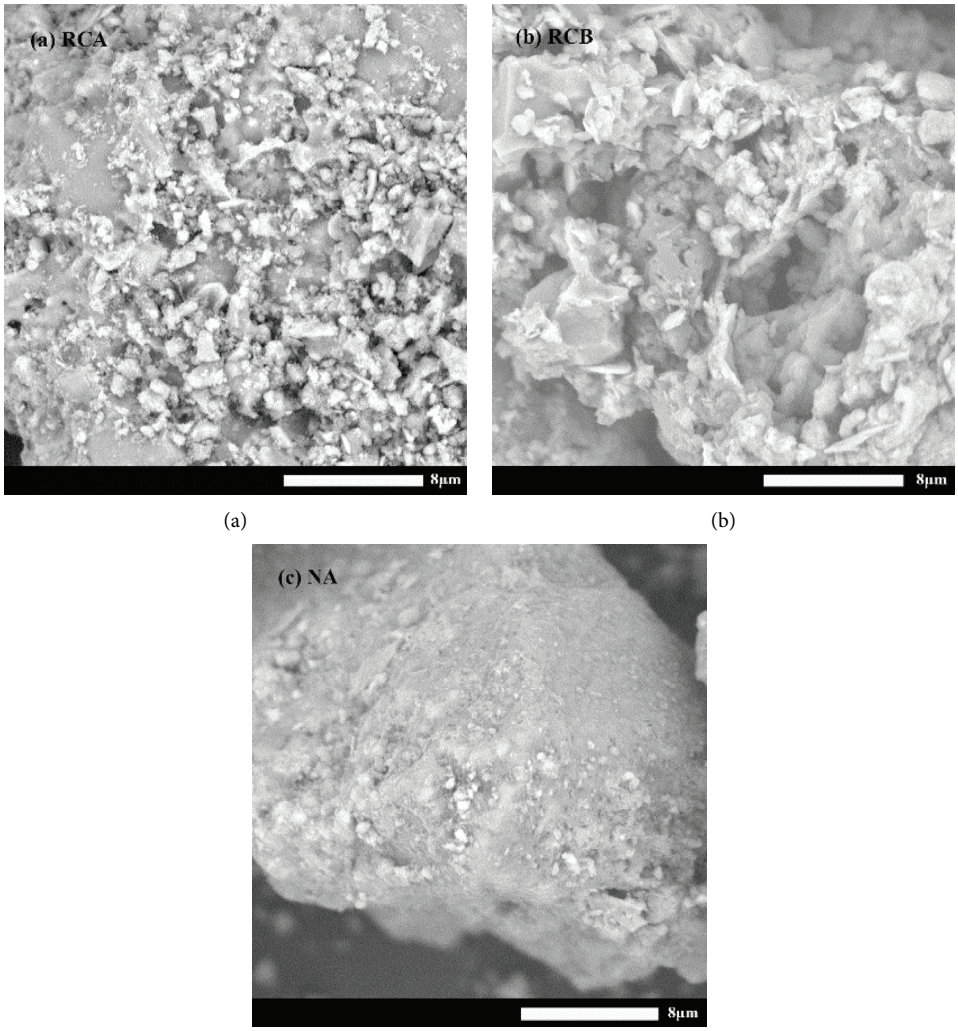

Figure 7: 10000×SEM image of RA and NA.

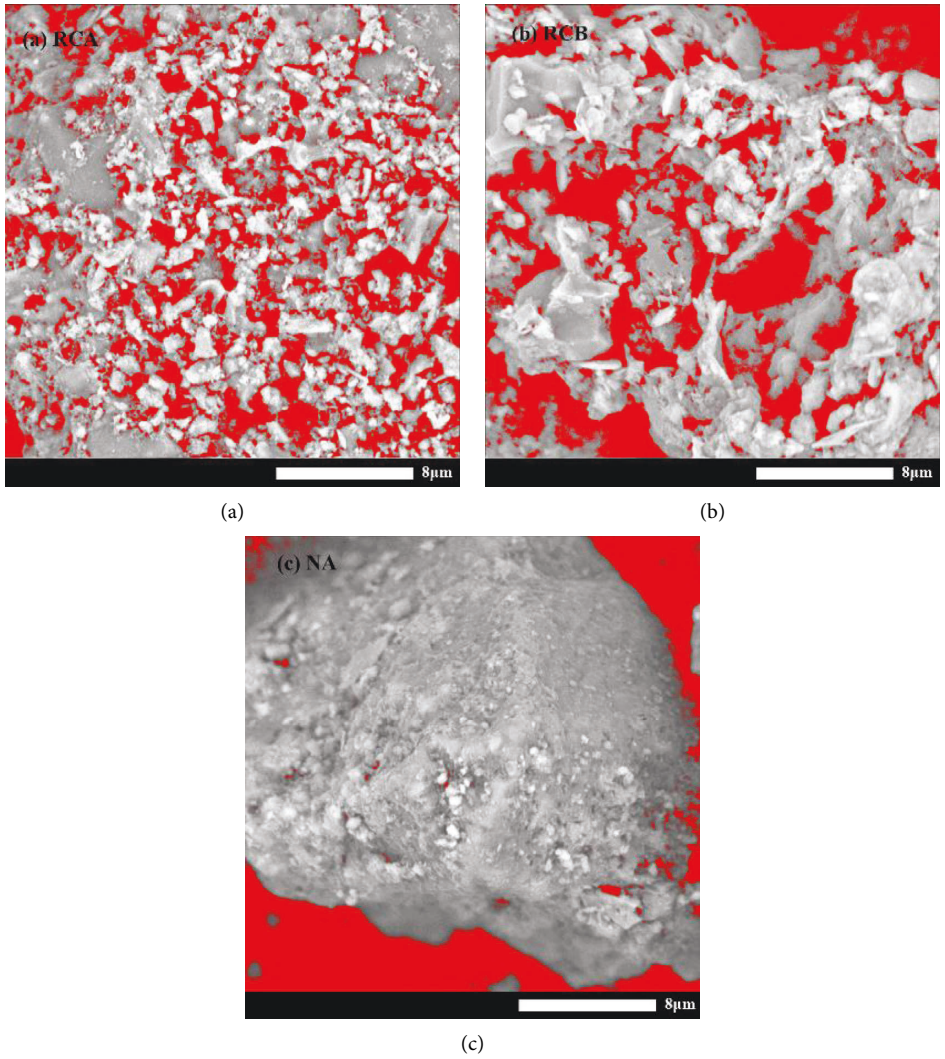

Figure 8: The binarization image of RA and NA.

Table 6: The porosity of RA and NA at different magnifications based on SEM images (%).

Magnifications	Types of RA		
	RCB	RCA	Natural aggregate
10000×	28.7	22.3	12.8
15000×	33.4	24.6	13.2
20000×	29.6	23.8	13.5
Average	30.6	23.6	13.2

magnification is smaller, resulting in the deviation between porosity and the actual value [3].

3.4. Quantitative Characterization and Evaluation of Contour Roughness of RA. RA is a complex porous aggregate. The microscopic pore structure, quantity, and size of roughness are one of the critical characteristics of microstructure parameters. The microscopic characteristics directly affect the basic indexes of raw materials, such as crushing value and water absorption, and indirectly affect the performance of cement stable reclaimed pavement, such as water pressure resistance, freezing resistance, permeability resistance, and shrinkage resistance.

Fractal theory is a new scientific theory proposed by Mandelbrot to describe image information. It quantifies the microscopic topography features by using a fractal dimension as a parameter, divides the set level from various perspectives, and measures the capacity of the system to fill space and the system's disorder [24]. The fractal dimension can be used as a quantitative analysis method for the roughness and microstructure of regenerated aggregates. There are many methods to calculate the fractal dimension, including box dimension, similarity

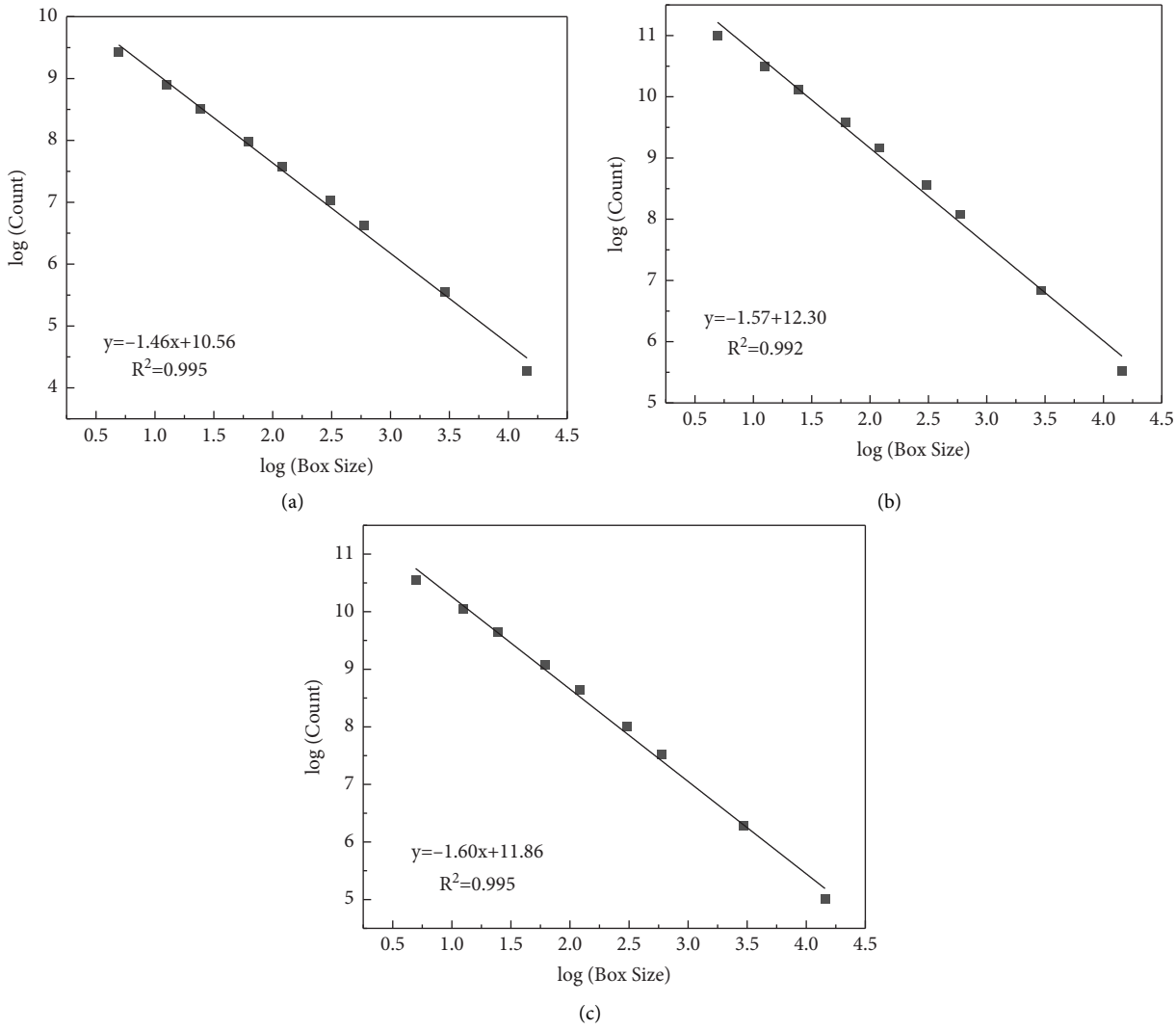

Figure 9: Box dimension of RA and NA. (a) NA, (b) RCA, and (c) RCB.

dimension, compass method, Minkowski method, variational method, perimeter area method, slit island method, and fractal Brownian model method. Box dimension is widely used because of its simplicity and practicality. For a fractal set F, we take a box of size r and cover F and write N (r) as the number of nonempty boxes. When we change the box size, N (r) will change, and when r⟶0, the fractal dimension can be obtained:

$$D = \lim_{r \longrightarrow 0} \frac{\ln N}{\ln r}. \quad (2)$$

The fractal dimension was calculated using the fractal box count plug-in in ImageJ software. First, an SEM image of 5000× was processed by using image-processing software, and the microcontour map of RA was obtained after binarization. Finally, the image was imported into ImageJ software for calculation and linear regression fitting. Thus, the fractal dimension of the image was obtained. The calculation results are shown in Figure 9.

It can be seen from Figure 9 and Table 7 that the correlation coefficients R^2 of different aggregates are 0.995, 0.992, and 0.995, respectively, indicating a good degree of fitting and obvious fractal characteristics [4]. The fractal dimension of different aggregates is RCB (1.6) > RCA (1.57) > NA (1.46). The box dimension of the SEM image reflects the pore characteristics and roughness of the microstructure, and the fractal dimension can evaluate the advantages and disadvantages of the microstructure. Previous studies have shown that in different fractal dimensions, the larger the fractal dimension, the worse the pore size and distribution uniformity and the more complex the microstructure, the larger the roughness [12, 13]. This also shows the difference in the microstructure between RA and NA from a quantitative point of view.

3.5. Analysis of the Strength Formation Mechanism of Regenerated Mixture. RCB and RCA were mixed according to different proportions of brick concrete, and the crushing value test was carried out as per the "Aggregate Test Regulations for Highway Engineering" (JTG E30-2005).

Table 7: Fractal dimension of RA and NA.

Aggregate types	Fitting equation	R^2	Fractal dimension
Natural aggregates	$y = -1.46x + 10.56$	0.995	1.46
RCA	$y = -1.57x + 12.30$	0.992	1.57
RCB	$y = -1.60 + 11.86$	0.995	1.60

It can be seen from Table 8 that to meet the requirement of crushing values of heavy traffic on the first-level highway in the Technical Rules for Construction of Highway Pavement Base (JTG/T F20 -- 2015), recycled aggregates with an RCB to RCA ratio of 2 : 8 are adopted. The median value of the C–B-3 grade is used for gradation, as shown in Figure 10.

As shown in Figure 11, increasing the dosage of construction waste decreases the maximum dry density mixture, and as a result, the best moisture content increases. According to the porosity analysis, RCB > RCA > NA is mainly due to the recycled aggregate of construction waste. Its internal surface has a lot of porosity and microcracks, and its surface is covered with a large number of cement mortars, which affect the mixture's properties. When the RA content increased from 0% to 100%, the maximum dry density decreased by 16% and the optimal moisture content increased by 50%.

As can be seen from Figures 12 and 13, with the increase in the RA content, 7d unconfined compressive strength and 7 d splitting strength of the mixture first increased and then decreased, reaching the peak value at 20% RA content. With the increase in the cement dose, force also increases. When the content of RA is less than 20%, along with the increase in the dosage of RA, the aggregate strength decreases. However, the surface of RA is coated with some mortar, which contains cement with incomplete hydration. Moreover, according to the analysis of RA components, RCA and RCB contain active silica and other substances. Due to the pozzolanic effect, higher strength and more stable calcium hydrate are generated, which improves the composition of hydrated cementing substances. Due to the small particle size, the packing effect occurs, which reduces the overall porosity and optimizes the pore structure and the performance of the interfacial transition zone. Due to the small particle size, the packing effect occurs, which reduces the overall porosity and optimizes the pore structure and the performance of the interfacial transition zone [25–32]. Second, in the mixing process of the mixture, because there are many pores in RA, absorbing more water is conducive to the hydration process of the water-stable specimen in the health period, generating more cement hydration products and improving the cohesion of the mixture [29]. Moreover, according to the fractal dimension of RA, RCB > RCA > NA, the contour of RA is rougher, which is also helpful in producing a more vital bonding force of cement mortars and improving the unconfined compressive strength and splitting strength of the mixture. When the RA content was greater than 20%, the bonding force between slurry and aggregates was already strong, and the strength improvement of bonding force could not make up for the strength reduction caused by high RA content, so the strength of the mixture decreased with the increase in the RA content.

Table 8: Crushing values of recycled aggregates with different proportions of brick concrete.

RCB: RCA	Measured values	Specification values	
		Base	Subbase
0 : 10	21.2		
2 : 8	25.3		
4 : 6	27.2		
5 : 5	28.3	≤26	≤30
6 : 4	32.1		
8 : 2	34.6		
10 : 0	37.2		

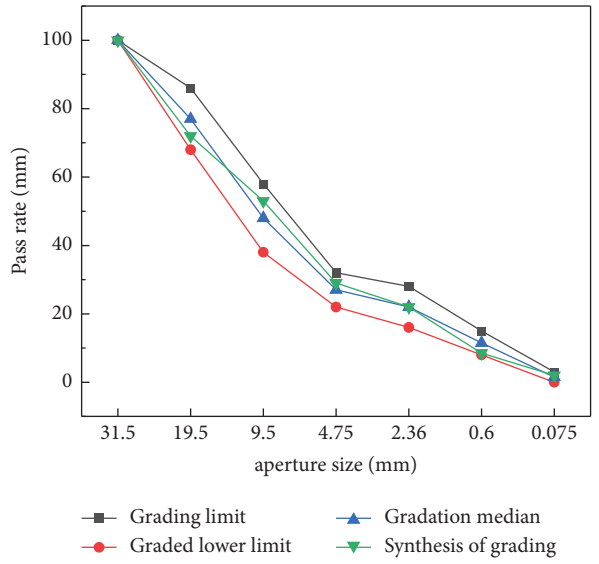

Figure 10: Grade distribution curve.

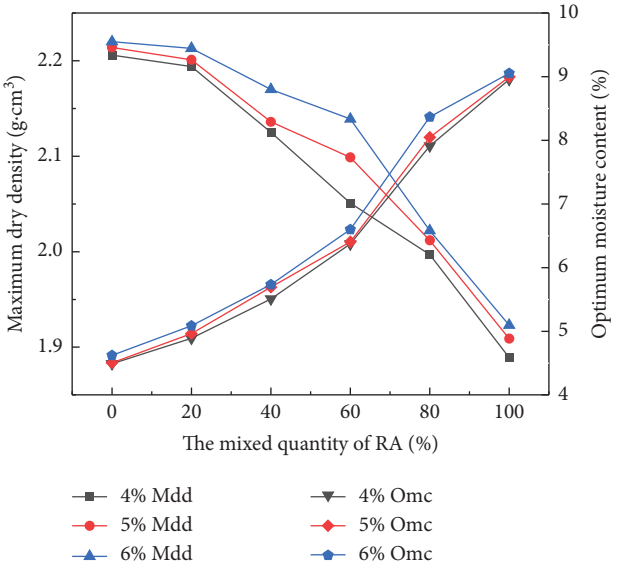

Figure 11: Maximum dry density and optimum moisture content of the recycled mixture.

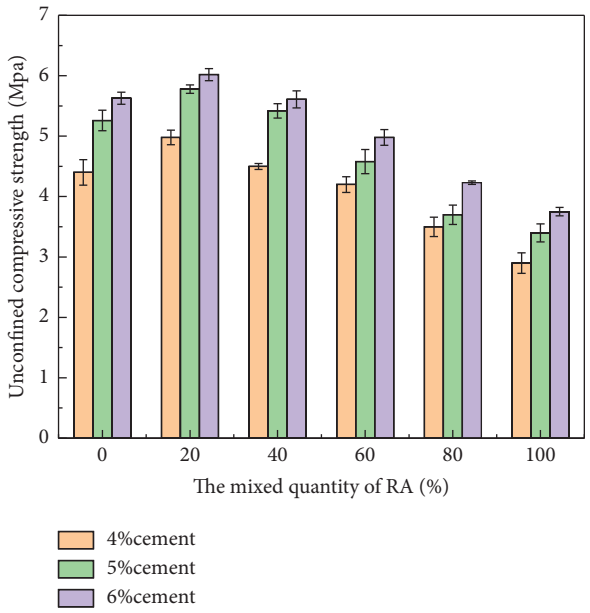

Figure 12: Unconfined compressive strength.

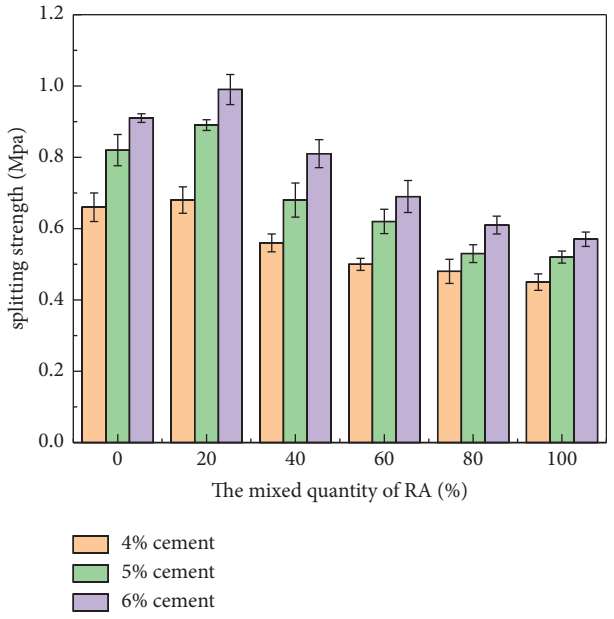

Figure 13: Splitting strength.

4. Conclusions

This study focuses on the composition, microstructure, and formation mechanism of construction waste, and the research conclusions are as follows:

(1) The mineral compositions of RA and NA were analyzed by EDS and XRD. The mineral compositions of RA and NA are pretty different.

(2) The porosity and fractal dimension of SEM images of RA and NA with different magnifications were calculated by ImageJ image processing technology. RA has prominent fractal characteristics, and its relationship is RCB > RCA > NA.

(3) The formation mechanism of the strength of the recycled mixture was analyzed. The maximum dry density of the mixture decreased with the mixing amount, and the optimal water content increased with the increase in the mixing amount. The variation trend of the mixture's unconfined compressive strength and splitting strength at 7 d is roughly the same, and the peak value exists at the RA content of 20%. The main reason is that RA's mineral composition and microstructure lead to the improvement of the bonding force between cement and aggregates, which makes up for the loss of aggregate strength, leading to the peak value. Appropriate RA content can be used for road bases and subbases to realize the resource utilization of construction waste in transportation. [33].

Data Availability

This research relies on the road construction project of K12 + 034-K13 + 034 low-quality construction waste recycling from Xiong'an New Area, S524, Hebei Province to Baoding. All data used to support the findings of this study are included in the article.

Conflicts of Interest

The authors declare that there are no conflicts of interest regarding the publication of this article.

Acknowledgments

This research was supported by the Natural Science Foundation of Hebei Province (E2018201106), the High-level Talents Funding Program of Hebei Province (B2017005024), and the Key Research Program of Education Department of Hebei Province (ZD2016073).

References

[1] J. H. Zhang, L. Ding, and A. S. Zhang, "Application of recycled aggregates from construction and demoliton waste in subgrade engineering: a review," *China Journal of Highway and Transport*, vol. 34, no. 10, pp. 135–154, 2021.

[2] Z. Li, L. L. Liu, S. H. Yan, M. Zhang, and Y. Xie, "Properties of microscopic particle morphology and particle contact of renewable construction waste mixtures," *Construction and Building Materials*, vol. 207, pp. 190–205, 2019.

[3] F. J. Qi, W. H. Sui, and G. L. Zhang, "Calculation and analysis of the porosity and fractal dimension of red stratum sandstone based on SEM images processing," in *Proceedings of the National Engineering Geology Academic Conference*, pp. 348–354, Beijing, China, November 2014.

[4] S. Gao, Q. Y. Li, and J. L. Luo, "Fractal characteristic of recycled aggregate and its influence on physical property of recycled aggregate concrete," *Reviews on Advanced Materials Science*, vol. 60, no. 1, pp. 663–677, 2021.

[5] J. F. Wu, L. B. Wang, and L. J. Meng, "Analysis of mineral composition and microstructure of gravel aggregate based on XRD and SEM," *Road Materials and Pavement Design*, vol. 18, no. sup3, pp. 139–148, 2017.

[6] J. Yang, Y. Su, X. Y. He et al., "Pore structure evaluation of cementing composites blended with coal byproducts: calcined coal gangue and coal fly ash," *Fuel Processing Technology*, vol. 181, pp. 75–90, 2018.

[7] L. Wang, M. M. Jin, Y. H. Wu, Y. Zhou, and S. Tang, "Hydration shrinkage, pore structure and fractal dimension of silica fume modified low heat Portland cement-based materials," *Construction and Building Materials*, vol. 272, Article ID 121952, 2021.

[8] L. Wang, Z. Yu, B. Liu, F. Zhao, S. Tang, and M. Jin, "Effects of fly ash dosage on shrinkage, crack resistance and fractal characteristics of face slab concrete," *Fractal and Fractional*, vol. 6, p. 335, 2022.

[9] Y. Wang, L. S. Li, M. Z. An, Y. Sun, Z. Yu, and H. Huang, "Factors influencing the capillary water absorption characteristics of concrete and their relationship to pore structure," *Applied Sciences*, vol. 12, no. 4, p. 2211, 2022.

[10] X. F. Wang, C. Chen, and Y. B. Wang, "Fractal analysis of porous alumina and its relationships with the pore structure and mechanical properties," *Fractal and Fractional*, vol. 6, no. 8, p. 460, 2022.

[11] T. Liu, X. N. Zhang, Z. Li, and Zq Chen, "Research on the homogeneity of asphalt pavement quality using X-ray computed tomography (CT) and fractal theory," *Construction and Building Materials*, vol. 68, pp. 587–598, 2014.

[12] J. Dai, S. L. Xu, and S. D. Song, "Changes in basalt before and after microwave irradiation based on XRD and SEM," *China Science Paper*, vol. 13, pp. 2780–2783, 2018.

[13] A. H. Farhan, A. R. Dawson, and N. H. Thom, "Characterization of rubberized cement bound aggregate mixtures using indirect tensile testing and fractal analysis," *Construction and Building Materials*, vol. 105, pp. 94–102, 2016.

[14] Q. Yun, P. C. Cai, and X. Li, "Quantitative characterization of macropore structure of granite residual soil," *Journal of Yangtze River Scientific Research Institute*, vol. 39, pp. 82–88, 2022.

[15] B. W. Kong, S.-H. He, Y. L. Tao, and J. Xia, "Pore structure and fractal characteristics of frozen-thawed soft soil," *Fractal and Fractional*, vol. 6, no. 4, p. 183, 2022.

[16] S. H. Zhang, Q. Y. Li, Q. Yuan, S. Yang, and X. Dai, "Effect of roughness on bonding performance between Portland cement concrete and magnesium phosphate cement concrete," *Construction and Building Materials*, vol. 323, Article ID 126585, 2022.

[17] Y. X. Peng, S. W. Tang, J. S. Huang, C. Tang, L. Wang, and Y. Liu, "Fractal analysis on pore structure and modeling of hydration of magnesium phosphate cement paste," *Fractal and Fractional*, vol. 6, p. 337, 2022.

[18] Z. Q. Yu and G. Ye, "The pore structure of cement paste blended with fly ash," *Construction and Building Materials*, vol. 45, pp. 30–35, 2013.

[19] K. Snehal, B. B. Das, and M. Akanksha, "Early age, hydration, mechanical and microstructure properties of nano-silica blended cementitious composites," *Construction and Building Materials*, vol. 233, Article ID 117212, 2020.

[20] J. Liu, Q. Qiu, F. Xing, and D. Pan, "Permeation properties and pore structure of surface layer of fly ash concrete," *Materials*, vol. 7, no. 6, pp. 4282–4296, 2014.

[21] T. Sinsiri, P. Chindaprasirt, and C. Jaturapitakkul, "Influence of fly ash fineness and shape on the porosity and permeability of blended cement pastes," *International Journal of Minerals, Metallurgy and Materials*, vol. 17, no. 6, pp. 683–690, 2010.

[22] D. Siang Ng, S. C. Paul, V. Anggraini et al., "Influence of SiO_2, TiO_2, and Fe_2O_3 nanoparticles on the properties of fly ash blended cement mortars," *Construction and Building Materials*, vol. 258, Article ID 119627, 2020.

[23] L. Wang, S. W. Tang, G. Pia, and E. Chen, "Editorial for special issue fractal and fractional in cement-based materials," *Fractal and Fractional*, vol. 6, no. 3, p. 144, 2022.

[24] Z. L. Yu, L. J. Zhao, and F. H. Meng, "Calculating SEM fractal dimension of concrete by MATLAB," *Cement Engineering*, vol. 5, pp. 59–62, 2014.

[25] J. H. Zhang, C. Li, L. Ding, and J. Li, "Performance evaluation of cement stabilized recycled mixture with recycled concrete aggregate and crushed brick," *Construction and Building Materials*, vol. 296, Article ID 123596, 2021.

[26] Q. F. Li and J. Hu, "Mechanical and durability properties of cement-stabilized recycled concrete aggregate," *Sustainability*, vol. 12, no. 18, pp. 7380–80, 2020.

[27] T. Meng, S. S. Lian, K. J. Ying, and H Yu, "Feasibility study of cement-stabilized materials using 100% mixed recycled aggregates from perspectives of mechanical properties and microstructure," *Reviews on Advanced Materials Science*, vol. 60, no. 1, pp. 490–502, 2021.

[28] J. L. Ren, S. Y. Wang, and G. Y. Zang, "Effects of recycled aggregate composition on the mechanical characteristics and material design of cement stabilized cold recycling mixtures using road milling materials," *Construction and Building Materials*, vol. 244, Article ID 118329, 2020.

[29] Z. Tian, *Performance of Cement Stabilized Crushed Stone Pavement Base Materials Containing Construction Waste*, Hunan University, Hunan, China, 2016.

[30] L. Q. Hu and A. M. Sha, "Performance test of cement stabilized crushed clay brick for road base material," *China Journal of Highway and Transport*, vol. 25, pp. 73–79, 2012.

[31] J. Xiao, C. F. Wu, and Z. H. Zhan, "Research on performance of cement stabilized brick and concrete recycled aggregate base," *China Journal of Highway and Transport*, vol. 30, pp. 25–32, 2017.

[32] M. L. Zeng, Z. Tian, and J. Xiao, "Performance of cement stabilized crushed stone pavement base materials containing construction waste," *Journal of Wuhan University of Technology*, vol. 38, pp. 34–38, 2016.

[33] P. Yong and J. J. Li, "Research on fractal dimension of construction waste under impact load," *Journal of North University of China (Natural Science Edition)*, vol. 43, pp. 254–259, 2022.